

Conjugate heat transfer in enclosures with openings for ventilation

E. Bilgen, T. Yamane

Abstract Conjugate heat transfer by natural convection and conduction in enclosures with openings has been studied by a numerical method. The enclosure contained a chimney consisting of a vertical solid wall, which was insulated on one side and a constant heat flux applied on the other. Vertical boundaries with openings were isothermal and horizontal boundaries adiabatic. These problems are encountered in heat transfer in buildings and heat management in electronic equipment. Two dimensional equations of conservation of mass, momentum and energy, with the Boussinesq approximation are solved using the Simpler method. Various geometrical parameters were: aspect ratio, A from 0.5 to 2.0, openings' heights, h_1 and h_2 from 0.10 to 0.30, orifice height, h_3 from 0.05 to 0.15, insulation thickness, w_1 from 0 to 0.10, wall thickness, w_2 from 0.05 to 0.15 and chimney width, w_3 from 0.05 to 0.15. Rayleigh number, Ra was varied from 10^8 to 10^{12} and the conductivity ratio, k_r was from 1 to 40. The results are reduced in terms of the normalized Nusselt number, Nu and volume flow rate, \dot{V} as a function of Ra number, and other non dimensional geometrical parameters. The isotherms and streamlines are produced for various Ra numbers and geometrical conditions. It is found that Nu and \dot{V} are both an increasing function of Ra , h_1 at high Ra numbers, h_3 , and k_r . They are a decreasing function of h_1 at low Ra numbers, h_2 , and w_2 . Nu and \dot{V} have optima with respect to w_1 , w_3 and A .

Nomenclature

A aspect ratio, H/L
 g acceleration due to gravity, m/s^2

h_1, h_2 opening heights, $h'_1/L, h'_2/L$
 h_3 orifice height, h'_3/L
 H enclosure height, m
 h convection coefficient, $W/m^2 \cdot K$
 k thermal conductivity, $W/m \cdot K$
 k_r thermal conductivity ratio, $k(solid)/k(fluid)$
 L enclosure width, m
 Nu Nusselt number, $\frac{hL}{k_f}$
 p' dimensional pressure
 P dimensionless pressure, $\frac{p'+\rho_0 g y'}{\rho_0 (\alpha_f/L)^2}$
 Pr Prandtl number, ν/α
 q dimensionless heat flux, $-\frac{\partial \theta}{\partial X}$
 q'' heat flux, W/m^2
 Ra Rayleigh number, $(g\beta q'' L^4)/(\nu\alpha k)$
 t' dimensional time, s
 t dimensionless time, $\frac{\alpha_f t'}{L^2}$
 T temperature, K
 u, v dimensional velocity in x and y direction
 U, V dimensionless velocity, $u'\alpha_f/L, v'\alpha_f/L$
 \dot{V} volume flow rate
 w_1, w_2 partition thickness, $w'_1/L, w'_2/L$
 w_3 chimney channel width, w'_3/L
 x', y' Cartesian coordinates
 X, Y dimensionless coordinates, $x'/L, y'/L$

Greek Letters

α thermal diffusivity, m^2/s
 β thermal expansion of fluid, $1/K$
 Γ general diffusion coefficient
 ψ stream function
 θ dimensionless temperature, $\frac{T-T_\infty}{(Lq''/k_f)}$
 μ dynamic viscosity, $kg/m \cdot s$
 ρ fluid density, kg/m^3
 ν kinematic viscosity, m^2/s

Superscripts

' dimensional variables
 – average

Subscripts

fluid
 r ratio
 s solid
 w wall
 ∞ reservoir
 1 section 1
 2 section 2

Received: 27 May 2002
 Published online: 16 April 2003
 © Springer-Verlag 2003

E. Bilgen, T. Yamane
 Shizuoka University,
 Faculty of Engineering, Hamamatsu, Japan,

E. Bilgen (✉)
 Ecole Polytechnique,
 University of Montreal,
 C.P. 6079, 'centre ville',
 Montreal, Qc, Canada, H3C 3A7
 E-mail: bilgen@polymtl.ca
 Tel.: +1-514-340-4711 ext. 4579
 Fax: +1-514-340-5917

We would like to express our sincere thanks to A. Nakayama and M. Kuwahara of Shizuoka University for helpful discussions and R. Ben Yedder of Ecole Polytechnique for valuable assistance in the computation using the mm code.

1 Introduction

Conjugate heat transfer by natural convection and conduction in open enclosures occurs in numerous practical situations, such as heat transfer in dwellings, window systems, solar collectors, rooms with fire spread, cooling of nuclear reactors, and heat management in electronic equipment (see, for example, [1]). In many applications, enclosures contain heat generating devices, which may have design restrictions to limit their temperatures. These problems are encountered, in particular, in passive cooling systems, for example, printed circuit board in an electronic cabinet and ventilation of dwellings. A literature review shows that although coupling of conduction and convection has been studied for various configurations [2], with fluid-porous media [3], [4], fluid-solid media [5], [6], there is rather little work with open enclosures relating to the above mentioned applications.

A literature review is carried out in these two areas of applications, which are directly related to the present study. In heat management applications, electronic components often flush mounted on boards are cooled by conduction and natural convection in enclosures. There is usually an upper limit for temperature allowed of these components and the heat management becomes an important aspect. A brief literature review shows that the case with enclosures having openings using natural, mixed convection and conduction has been studied in a few studies [7]–[11].

Du et al. [7] studied mixed convection heat transfer in vertical channels open at the bottom and top, with protruding discrete heaters installed on one side. They found that the cooling of the electronic components was affected by the imposed flow, the strength of the natural convection, the aspect ratio and their position in the channel. Thermal management of a tape ball array package, which was attached to a plate and placed in a channel was studied by Sathe and Sammakia [8]. They used a three dimensional conjugate heat transfer model to evaluate various parameters' effects on the chip junction temperatures. They showed good agreement with experimental results and importance of radiation heat transfer in thermal management. Harman and Cole [9] studied conjugate heat transfer problem with two-layer substrate. They considered a horizontal system of infinite lateral extent with a flush mounted heater generating heat uniformly. The top layer was subjected to a shear flow, and the radiation and natural convection were neglected. They used an analytical-numerical approach to solve governing equations and derived appropriate design correlations. More complex geometrical problems have also been studied. For example, Thrasher et al. [10] studied experimentally a thermal system which consisted of pin-fin heat sink and chimney. They studied the effect of various parameters, namely, porosity, pin spacing and pin numbers on the heat transfer and showed good agreement with the theoretical results of a previous study. Jilani et al. [11] performed a numerical analysis to study heat management of a flush mounted electronic component installed in an enclosure with a single opening. They investigated, at small Rayleigh

numbers, the effects of heat flux, opening size and in and out going air flow from the opening on the heat transfer.

The direct and indirect solar chimney principle has been used for heating of dwellings, drying of crops, dehumidification of air and as cooling tower (see, for example, [12]). In heating applications, for example, the dwelling is simulated as an enclosure having a solar chimney located towards the sun, which serves as a receiver of the solar radiation and also serves as an energy storage device. The dwelling air enters the chimney from orifices on its lower part, it is heated in the chimney as a result of which it rises and is returned to the dwelling through openings on the top. The air circulates in the dwelling, even after the sunset due to heat accumulated, in part, in the storage device, which is usually a massive wall. In this case, the heat is released from the surface of massive wall as if it had a flush mount heat source on it (see, for example, [13]). The same principle may also be used for space ventilation. In this case, dwellings have openings in opposite sides, the solar chimney is located towards the sun and serves as a heat source to drive the air. It enters from outside through openings opposite to the solar chimney and exits from openings at the top of it. The literature review shows that there is quite a few studies on heating applications (see for example, [4]) but none on the cooling and ventilation.

The previous studies clearly indicate that the chimney concept has interesting applications in both fields. The heat transfer by natural convection and conduction in passive systems constitutes a major study area. Depending on the applications and aims to be achieved, various interactions between convection and conduction should be known, the governing parameters and their effects on the thermal performance should be established. The aim of this study is to examine the interaction between the conduction in the solid wall and convection in the fluid, and the effects of an insulation layer on the solid wall, and various geometrical parameters, such as openings size, which influences the fluid flow rate.

2 Problem description

A schematic of the two dimensional system with geometrical and boundary conditions is shown in Fig. 1. Constant heat flux, q'' is released from the wall facing the right boundary, which is transferred by conduction through the solid wall and by natural convection to a fluid circulating through the chimney and the opening on the top right hand side. The fluid is discharged to the fluid reservoir at a characteristic temperature T_∞' . The circulating fluid enters the enclosure from the opening on the top left hand side, although some re-circulation at both openings may occur. Vertical boundaries are in contact with the same fluid reservoir, hence at T_∞' . Horizontal boundaries of the enclosure are insulated hence, adiabatic.

Although the geometrical size of these systems in different applications may be different, the non-dimensional scales are usually similar: the enclosure aspect ratio, $A \approx 0.5$ to 2 , the openings and channels, $h \approx 0.05$ to 0.30 , partition wall thickness and channel width, $w \approx 0$ to 0.15 ,

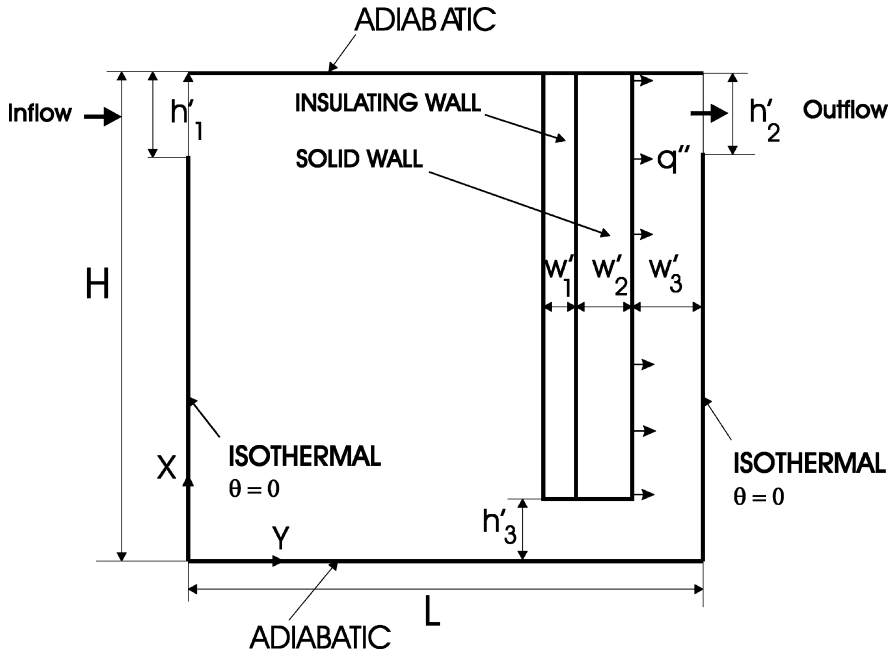


Fig. 1. Geometry and boundary conditions of the problem

the conductivity ratio $k_r \approx 1$ to 40 and the heat flux from the heat source, $q'' \approx 10^3$ to 10^6 W/m².

3 Mathematical model

Continuity, momentum and energy equations for laminar flow of an incompressible Newtonian fluid in two dimensional geometry are used to model the heat transfer. Following assumptions are made: there is no viscous dissipation, the gravity acts in the vertical direction, fluid properties are constant and fluid density variations are neglected except in the buoyancy term (the Boussinesq approximation) and radiation heat exchange is negligible. Using non-dimensional variables defined in the nomenclature, the non-dimensional governing equations are obtained as

$$\frac{\partial U}{\partial X} + \frac{\partial V}{\partial Y} = 0 \quad (1)$$

$$\frac{\partial U}{\partial t} + U \frac{\partial U}{\partial X} + V \frac{\partial U}{\partial Y} = -\frac{\partial P}{\partial X} + \Gamma Pr \nabla^2 U \quad (2)$$

$$\frac{\partial V}{\partial t} + U \frac{\partial V}{\partial X} + V \frac{\partial V}{\partial Y} = -\frac{\partial P}{\partial Y} + \Gamma Pr \nabla^2 V + Ra Pr \theta \quad (3)$$

$$\frac{\partial \theta}{\partial t} + U \frac{\partial \theta}{\partial X} + V \frac{\partial \theta}{\partial Y} = k_r \nabla^2 \theta \quad (4)$$

where Γ is a general diffusion coefficient and 1 in the fluid region and 10^{15} in the solid region, k_r is 1 in the fluid region and k_s/k_f in the solid region. Γ and k_r are introduced in the equations to ensure $U = V = 0$ everywhere including at the solid-fluid interface and the conduction is accounted for in the solid region.

Average and normalized Nusselt numbers are calculated respectively as

$$\left. \begin{aligned} \overline{Nu} &= \frac{1}{A} \int_0^A \left(-\frac{\partial \theta}{\partial X} + U \theta \right) dY \\ Nu &= \frac{\overline{Nu}_{Ra}}{\overline{Nu}_{Ra=0}} \end{aligned} \right\} \quad (5)$$

The volume flow rate is calculated as

$$\left. \begin{aligned} \dot{V} &= - \int_{X=1} U_i dY \\ U_i &= U_{X=1} \quad \text{if } U_{X=1} < 0, \quad U_i = 0 \quad \text{if } U_{X=1} \geq 0 \end{aligned} \right\} \quad (6)$$

The stream function is calculated from its definition as

$$U = -\frac{\partial \psi}{\partial Y}, \quad V = \frac{\partial \psi}{\partial X} \quad (7)$$

where ψ is zero on the solid surfaces and the streamlines are drawn by $\Delta \psi = (\psi_{max} - \psi_{min})/n$ with n =number of increments.

4 Numerical technique

The computational domain was restricted to the enclosure with the wall. Hence, the boundary conditions are (see Fig. 1)

$$\left. \begin{aligned} U &= 0, V = 0 \text{ on the solid surfaces} \\ \frac{\partial \theta}{\partial Y} &= 0 \text{ on the horizontal boundaries} \\ \theta &= 0 \text{ on the vertical boundaries} \\ q &= -\frac{\partial \theta}{\partial X} \text{ on the wall facing the right hand side boundary} \\ P &= 0, \frac{\partial V}{\partial X} = 0, \left(\frac{\partial \theta}{\partial X} \right)_{out} = 0, \theta_{in} = 0 \text{ at the openings} \end{aligned} \right\} \quad (8)$$

The numerical method used to solve Eqs. (1) to (4) is the Simpler (Semi-Implicit Method for Pressure Linked Equations Revised) algorithm [14]. The computer code based on the mathematical formulation discussed earlier

and the Simpler method have been validated for various cases published in the literature, the results of which are discussed elsewhere [6], [15]. Uniform grid in the solid and non-uniform grid in the cavity were used for all computations. Grid sizes were varied depending on the geometrical condition. For example, for $A=1$, it was 60×60 (32 in the left part of the enclosure + 7 each in solid walls + 14 in the chimney channel).

Grid convergence was studied for a square enclosure. Grid sizes from 20×20 to 90×90 were tried. Grid independence was achieved within 1.1 percent with a grid size of 60×60 . Similar tests were conducted with enclosures having $A = 0.5$ and 2.0 and the grid size was adjusted accordingly. The execution time for a typical case with $A = 1$, the grid size of 60×60 , $Ra = 10^{10}$ and for 1800 iterations was 1380 s using a P.C. with 1.50 GHz clock speed.

The accuracy control was carried out by the conservation of mass by setting its variation to less than 10^{-3} , on the pressure term by setting the variation of residues at 10^{-3} . In addition, the accuracy of computations was checked using the energy conservation within the system, by setting its variation to less than 10^{-4} .

5 Results and discussion

Flow and temperature fields are examined. Geometrical parameters were: aspect ratio $A = 0.5$ to 2.0 , insulation thickness, $w_1 = 0$ to 0.10 , solid wall thickness $w_2 = 0.05$ to 0.15 , chimney channel width, $w_3 = 0.05$ to 0.15 , openings $h_1 = h_2 = 0.10$ to 0.30 , and orifice height, $h_3 = 0.05$ to 0.15 . Thermal parameters were: solid wall conductivity ratio, k_r (solid) = 1 to 40 , insulation conductivity ratio k_r (insulation) = 1 , and $Pr = 0.72$ (for air). It is noted that the lower limit of the conductivity ratio corresponds to an insulating wall having its thermal conductivity equal to that of air. In fact, polystyrene rigid (extruded), urethane (two-part mixture) and rigid foam, for example, all have almost the same thermal conductivity as that of air at ambient temperature. The Rayleigh number was varied from 10^8 to 10^{12} . First, flow and temperature fields, and the heat transfer and circulation flow rate will be examined for the base case, which is with $A=1$, $h_1 = h_2 = 0.10$, $h_3 = 0.05$, $w_1 = w_2 = 0.05$, $w_3 = 0.10$ and $k_r = 40$. Later, the effects of these parameters on the thermal performance of the system will be presented and discussed. In streamline and isotherm plots, the number of increment is $n=12$ for Ψ and 7 for θ .

6 Base case: general observation

The streamlines and isotherms in the computation domain for the base case for $Ra = 10^8$, 10^{10} and 10^{12} are presented in Fig. 2. At low Rayleigh number, Fig. 2(a), the streamlines on the left show a single cell and they are regularly spaced and well coordinated with $\Psi_{max} = 7.58$ ($X=0.44$, $Y=0.57$) and $\Psi_{min} = -0.25$ ($X=1$, $Y=0.94$). There is an anti-clockwise circulation on the left part of the enclosure and a weak clockwise circulation at the top of the chimney. Mass transfer from the left opening is weak. Isotherms on the right show a quasi-conduction regime; there is a stratification in the left enclosure. At higher Rayleigh number,

$Ra = 10^9$, formation of one cell was also observed, and it was connected to the opening at the left. The streamlines showed basically a similar trend, but the strength of circulation had increased; it was noticed that the center of the anti-clockwise cell had shifted towards left of the enclosure ($\Psi_{max} = 17.32$ ($X=0.25$, $Y=0.28$)). The clockwise circulation in the chimney was at the same location as before but its strength had increased about six folds, with $\Psi_{min} = -1.49$ ($X=1$, $Y=0.94$).

At $Ra=10^{10}$, Fig. 2(b) shows that the circulation is more vigorous with two cells circulating in the left part of the enclosure: the anti-clockwise cell filling almost all the enclosure is slightly skewed and Ψ_{max} is 62.08 ($X=0.56$, $Y=0.38$); the second, a clockwise circulating cell is connected to the left opening and its strength is weaker with respect to the first, with $\Psi_{min} = -22.3$ ($X=0.20$, $Y=0.60$). The isotherms show quite steep gradients at the solid wall surfaces and stratification in the enclosure. Both figures are indications of a strong circulation through the openings and increased mass transfer from left to right. A similar observation was made when Ra was increased further. At $Ra=10^{11}$, the strength of circulation of the first cell had increased to $\Psi_{max} = 101.60$ ($X=0.56$, $Y=0.67$), its center had shifted upwards, at the same time, the second cell had occupied left lower part of the enclosure also with increased strength, with $\Psi_{min} = -44.08$ ($X=0.24$, $Y=0.26$). The isotherms had showed a similar trend to those of $Ra=10^{10}$.

At $Ra = 10^{12}$ in Fig. 2(c), it is seen that the convection is vigorous with $\Psi_{max}=241.23$ ($X=0.6$, $Y=0.86$) and $\Psi_{min}=-244.40$ ($X=0.40$, $Y=0.40$). The first anti-clockwise cell is moved further upwards, and the second clockwise cell occupies almost the entire enclosure on the left part. Both are connected to the left reservoir through the opening, indicating a strong mass transfer. The isotherms show steep gradients on the solid surfaces, especially in the chimney.

7 Base case: Heat transfer and circulation flow rate

The normalized Nusselt number, Eq. (5), which expresses the heat transfer from the heat source, and the circulation flow rate \dot{V} are presented next as a function of Rayleigh number, Ra , in Fig. 3. In Fig. 3, and subsequent figures, Nu_1 and Nu_2 are the normalized Nusselt number through the left and right vertical boundaries respectively. As expected, we can see that the heat transfer at both boundaries increase with increasing Rayleigh number. At $Ra=10^8$, as observed earlier with Fig. 2a, the heat transfer is by quasi-conduction, especially through the right hand side, because of weak fluid circulation. The situation on the left is also similar but there is an indication of convection. As the Rayleigh number increases to 10^9 and 10^{10} range, the heat transfer by convection becomes a dominant mode, more so through the left boundary. Thereafter the heat transfer becomes a steady increasing function of Rayleigh.

Following our observation with Fig. 2 and the heat transfer results in Fig. 3, we see that the volume flow rate or mass transfer through the openings is an increasing function of Rayleigh, first with a steep increase from $Ra = 10^8$ to 10^9 . This may be due to transition from quasi-conduction to convection regime. As observed earlier with Fig. 2a, the volume flow rate is very weak at $Ra = 10^8$,

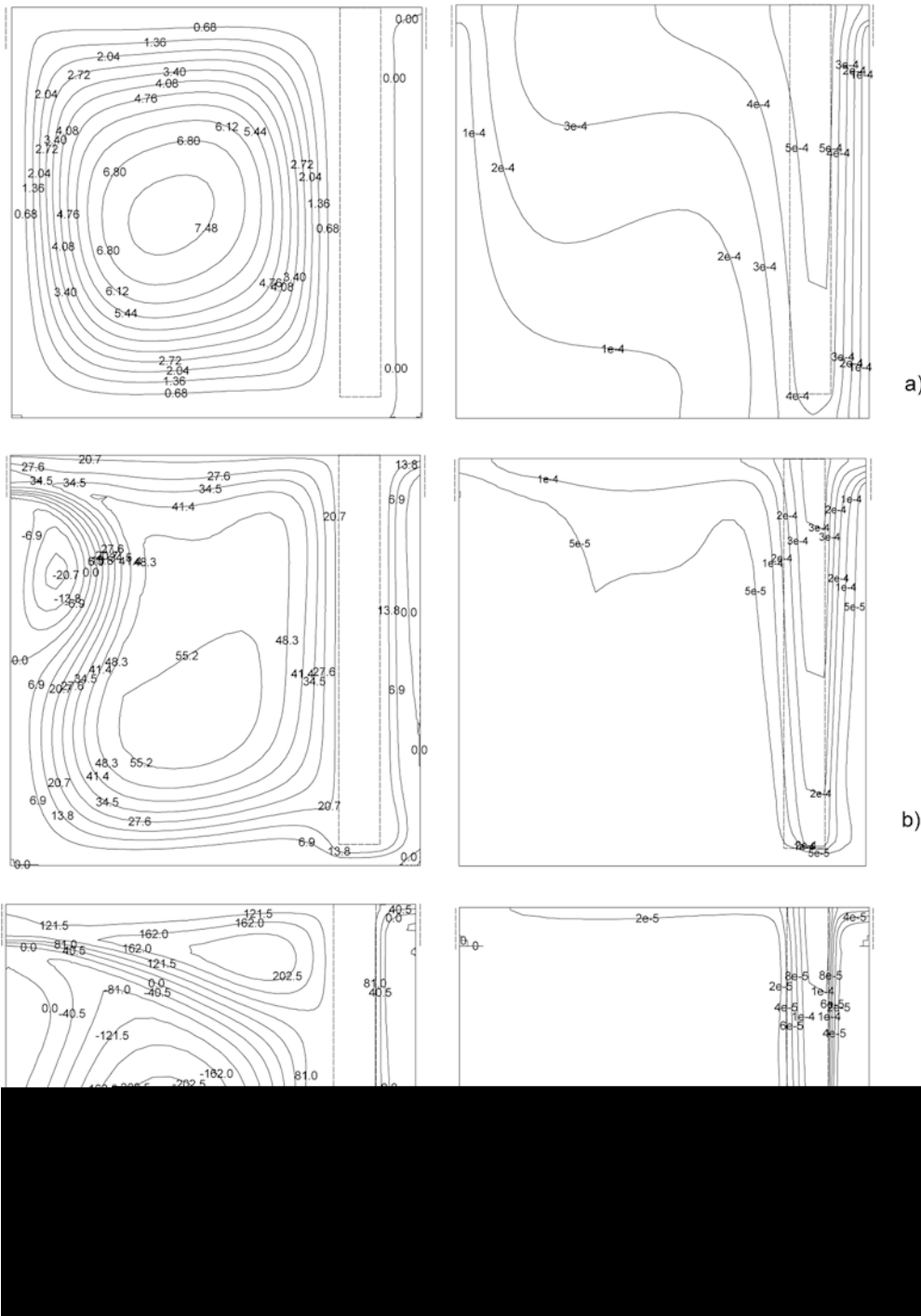


Fig. 2. Streamlines (on the left) and isotherms (on the right) for the base case of an enclosure with $A=1$, $h_1=h_2=0.10$, $h_3=0.05$, $w_1=w_2=0.05$, $w_3=0.10$ and $k_r=40$. The composite solid wall in the enclosure is shown with dashed line. The openings on the left, h_1 and on the right, h_2 are shown on the upper part of the enclosure with dashed lines. a) $Ra=10^8$, b) $Ra=10^{10}$, c) $Ra=10^{12}$

which increases one order of magnitude when $Ra = 10^9$. Beyond $Ra = 10^{10}$, the mass transfer increases steadily with increasing Rayleigh number. We observe that at high Rayleigh numbers there is a steady circulation of the fluid through the openings, which is essential for a successful heat management.

8 Effects of openings and orifice

A priori, the openings at left and right, h_1 and h_2 , and the orifice, h_3 , are important parameters, since they control the flow rate of fluid through the enclosure by restricting

it. By a parametric study, we would like to establish the importance of each on the heat transfer and fluid flow rate. We present first the streamlines and isotherms by varying each parameter h_1 , h_2 and h_3 while keeping the other two constant in Fig. 4. Then we present their respective heat transfer and flow rates for $Ra = 10^{10}$ to 10^{12} in Fig. 5.

Fig. 4 shows the streamlines (on the left) and isotherms (on the right) for $h_1 = h_2 = 0.3$ and $h_3 = 0.15$ at $Ra = 10^{10}$, which may also be compared with the base case. We can observe in Fig. 4a that when the opening on the left hand side is increased by three times while keeping the other two at their base values, the circulation pattern in the left

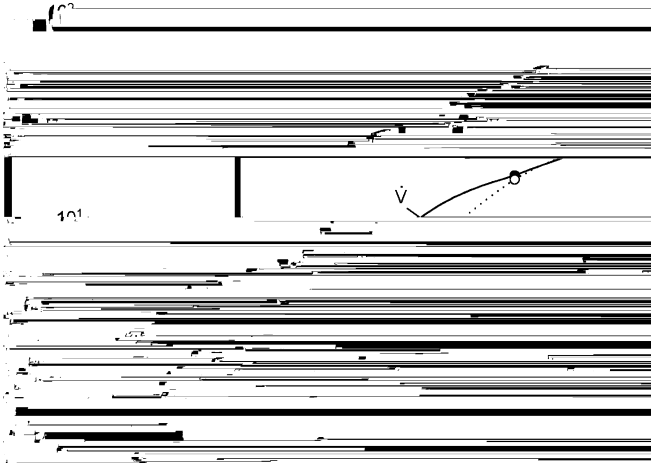


Fig. 3. Normalized Nusselt number and flow rate as a function of Rayleigh number for the base case

part of the enclosure becomes radically changed with formation of an anti-clockwise rotating cell at the upper part and a clockwise rotating cell at the lower part of the enclosure. The strength and coordinates of circulation in these cells, $\Psi_{max} = 61.94$ ($X=0.60, Y=0.79$) and $\Psi_{min} = -34.30$ ($X=0.35, Y=0.33$), show that with respect to the base case, Fig. 2b, the anti-clockwise rotating cell has almost the same strength but shifted upwards, and the new clockwise rotating cell occupying the lower part has a considerable strength, restricting the fluid flow. Indeed, the situation with $h_1 = 0.20$ for this case had a similar appearance and strength of circulation as that of Fig. 4a. Therefore the effect of h_1 on the heat transfer and flow rate is expected to be moderate, which is indeed the case in Fig. 5a. We see that at $Ra = 10^{10}$, although Nu_1 has increased by a few percent with h_1 , Nu_2 as well as volume flow rate, \dot{V} , are almost the same. The reason for the enhanced heat transfer through the left is of course due to heat transfer by the anti-clockwise rotating cell, which is in contact with the wall support system.

Generally, we observe a similar trend at higher Rayleigh numbers: Fig. 5a shows that Nu_1 and \dot{V} increase by about 3 and 7% respectively as h_1 increases from 0.1 to 0.3 for $Ra = 10^{12}$. The variation of Nu_2 is however more discernible, with about 20% for the same situation.

Fig. 4b shows streamlines and isotherms at $Ra = 10^{10}$ and for the case of $h_2 = 0.30$ with all the other parameters being the same as in the base case. We see that the streamlines and isotherms are similar to the base case, Fig. 2b. There are two counter rotating cells, their strength and coordinates are $\Psi_{max} = 56.52$ ($X=0.48, Y=0.38$) and $\Psi_{min} = -21.26$ ($X=0.11, Y=0.71$). Compared to the base case shown in Fig. 2b, the strength of the counter clockwise cell has increased considerably, choking the fluid flow in the system. The isotherms show slightly increased temperature gradients in the chimney. Indeed, Fig. 5b shows that the flow rate and heat transfer at $Ra = 10^{10}$ are both a decreasing function of h_2 . The decrease is over 25% in \dot{V} and Nu_1 , and 20% in Nu_2 when the opening on the right is increased from 0.1 to 0.3. For higher Rayleigh numbers, a reduced fluid flow rate and heat transfer is more discernible. The relative decrease is 35% in \dot{V} and

Nu_1 at $Ra = 10^{11}$ and 43% and 30% at $Ra = 10^{12}$. Heat transfer to the right, Nu_2 , follows a similar trend.

The effect of orifice size for the same Rayleigh number is shown in Fig. 4c, where the orifice size is increased by three times, but all the other parameters are the same as in the base case. Similar to that of Fig. 2b, streamlines show two counter rotating cells in the left enclosure. The strength of the clockwise rotating cell has decreased a little, that of the counter clockwise rotating cell filling the entire enclosure has increased a little: strength and coordinates are $\Psi_{max} = 66.45$ ($X=0.52, Y=0.34$) and $\Psi_{min} = -29.45$ ($X=0.14, Y=0.63$). Isotherms near the heat source show steeper gradients. Fig. 5c show that \dot{V} , Nu_1 and Nu_2 are all increasing function of h_3 . At $Ra = 10^{10}$, the increase is 30% in \dot{V} , Nu_1 and it is 26% in Nu_2 . As the Rayleigh increases, these variations become 15% at $Ra = 10^{11}$ and 8% at $Ra = 10^{12}$. This trend may be explained by examining the velocity profiles at openings. For the base case and at $Ra = 10^8, 10^{10}$ and 10^{12} they are traced and shown in Fig. 6. Following our observations with Fig. 2, we see that at $Ra = 10^8$, there is not much flow through these sections, showing that the heat transfer is by conduction only. For $Ra = 10^{10}$ and 10^{12} , Fig. 6a and 6b show that the fluid flows at the center from left to right and in the upper and lower parts there is a back flow. As expected, their magnitudes are an increasing function of Rayleigh number. Fig. 6c shows that the flow is from left to right without a back flow. It is seen that the back flow at section 1 and 2 becomes a controlling parameter in heat management. As Ra is increased, the back flow becomes relatively more important.

9 Effects of wall and insulation thickness, and chimney width

The insulation thickness was varied from 0 (for no insulation) to 0.10. The results for $Ra = 10^{10}$ to 10^{12} are presented in Fig. 7a. We see that fluid flow rate, \dot{V} and heat transfer, Nu_1, Nu_2 are first an increasing function of w_1 and then a decreasing function. With no insulation on the wall, a part of the heat is transferred by conduction to the left hand side and dissipated by convection. It was seen that the fluid flow was choked by counter rotating cells formed in the left enclosure, as a result of which heat transfer is reduced. As the insulation thickness is increased, the heat transfer in the chimney increases, promoting a better fluid circulation through the chimney. Depending on the Rayleigh number there seems to be an optimum insulation thickness, around $w_1 \approx 0.05$. The improvements are over 35 and 55% in \dot{V} , 55 and 66% in Nu_1 , and 35 and 55% in Nu_2 at $Ra = 10^{11}$ and $Ra = 10^{12}$ respectively.

The effect of the wall thickness, w_2 on Nu_1, Nu_2 and \dot{V} is shown in Fig. 7b. We can see that the fluid flow rate and heat transfer are not too sensitive to w_2 at low Rayleigh numbers, but variation is considerable at high Rayleigh numbers. For example, by increasing the wall thickness by three times, \dot{V} , Nu_1 and Nu_2 decrease by 17, 24, 20% at $Ra = 10^{11}$ and 25, 32, 26% at $Ra = 10^{12}$ respectively. By examining the streamlines and isotherms, we saw that the reason for this decrease was due to higher thermal resistance to heat flow through the wall, as a result of which the convection on the left part of the enclosure was reduced, affecting fluid flow through the chimney.

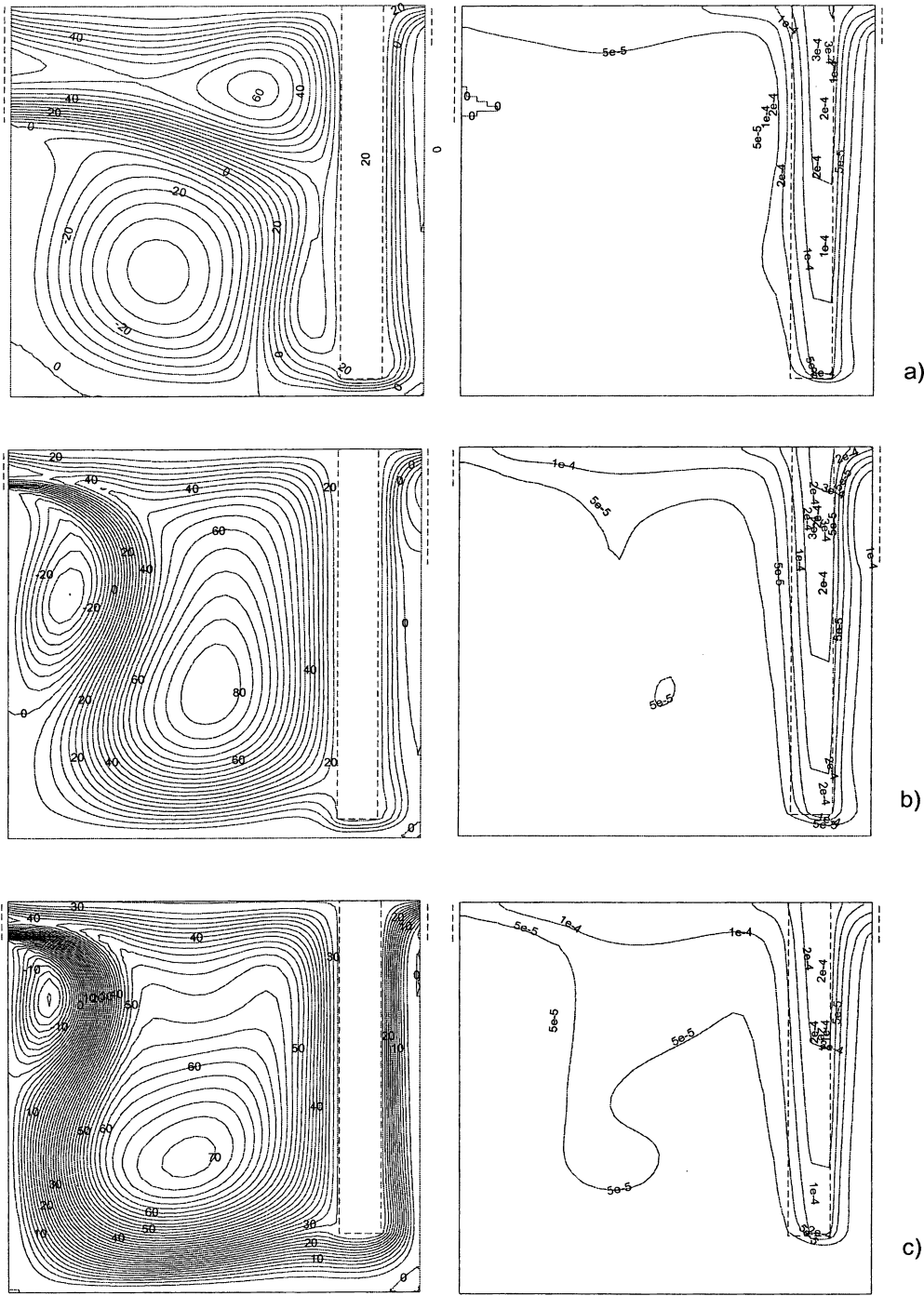


Fig. 4. Streamlines (on the left) and isotherms (on the right) for the base case at $Ra=10^{10}$ with h_1 , h_2 and h_3 parameters. The composite solid wall in the enclosure is shown with dashed line. The openings on the left, h_1 and on the right, h_2 are shown on the upper part of the enclosure with dashed lines. a) $h_1=0.30$, b) $h_2=0.30$, c) $h_3=0.15$

A priori, the chimney width is an important parameter, which would affect the flow rate and heat transfer, because the heat source is located in it. Fig. 7c shows Nu and \dot{V} as a function of w_3 for Ra from 10^{10} to 10^{12} . The flow rate goes through a maximum at each Ra . Since it is connected to the enclosure on the left, the effect of w_3 on the flow rate is influenced by the situation there. We can see that for small w_3 , \dot{V} is relatively smaller and it increases with increasing w_3 , and then decreases due to choking effect of the cells in the cavity on the left, as we observed earlier. As expected, the heat transfer through the left, Nu_1 follows a similar trend. The heat transfer through the right, Nu_2 however has a

mixed pattern: it goes through a maximum at low Rayleigh numbers but through a minimum at high Rayleigh numbers. It was seen that Nu_2 plotted with respect to Ra showed a mixed pattern with w_3 as parameter: at low Rayleigh numbers, the heat transfer was dominated by conduction regime when the channel width was small and by convection when it was large. Hence, Nu_2 was an increasing function of w_3 . At Ra between 10^{10} and 2×10^{11} , Nu_2 varied with a steeper slope when w_3 was smaller, as a result of which above $Ra = 2 \times 10^{11}$ Nu_2 became a decreasing function of w_3 . A similar trend was observed with the flow rate, \dot{V} , when plotted similarly, showing that the observed phenomenon was related to the strength and type of the convection in the cavity on the left.

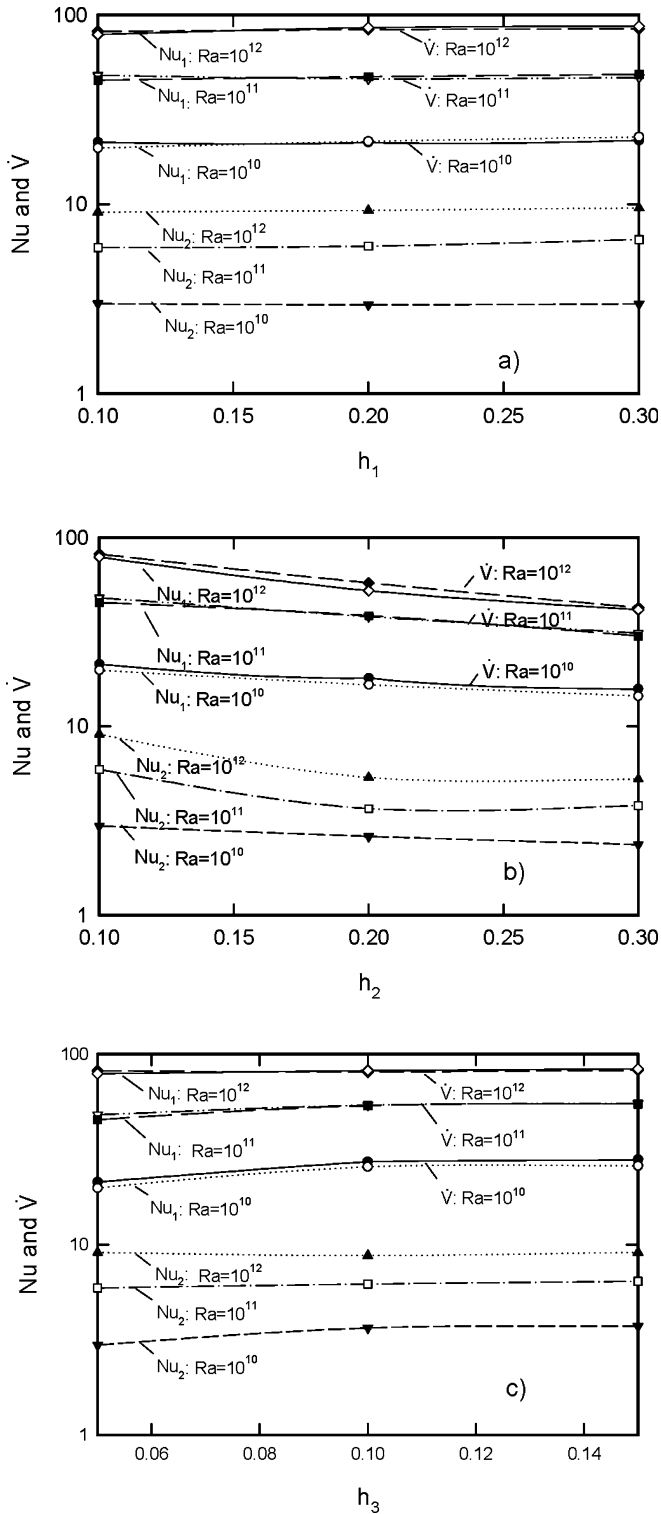


Fig. 5. Normalized Nusselt number and volume flow rate as a function of openings, a) h_1 , b) h_2 , and the orifice c) h_3 . They are for the base case and $Ra = 10^{10}$ to 10^{12}

10 Effect of conductivity ratio

The effect of conductivity ratio was studied by varying it from 1 to 40. The streamlines and isotherms for $Ra=10^{12}$ are presented in Fig. 8, which may be compared

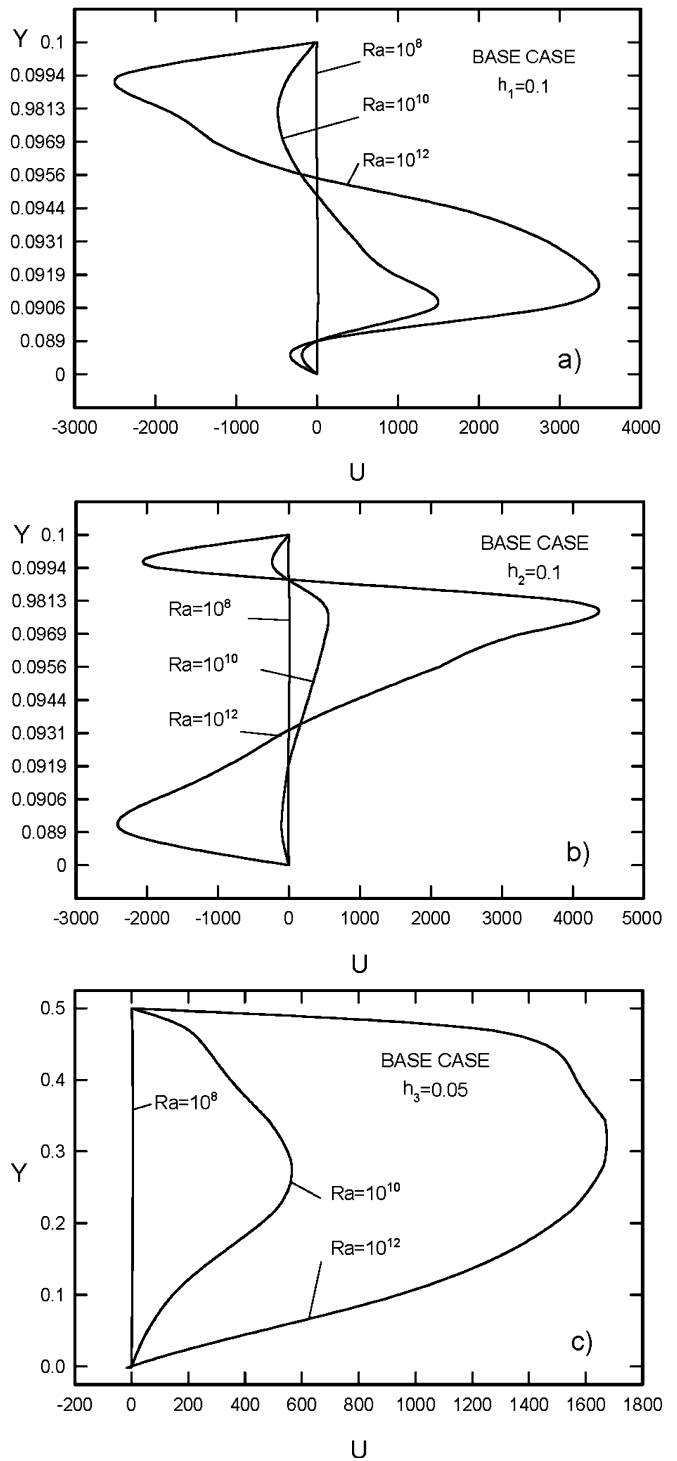


Fig. 6. Velocity profiles at the openings for the base case, a) h_1 , b) h_2 , and at the orifice, c) h_3 for the base case and $Ra = 10^{10}$ to 10^{12}

with the base case with $k_r=40$ of Fig. 2c. We see that for $k_r=1$, there are three counter rotating cells on the left side of the enclosure and the main anti-clockwise rotating cell is pushed all the way up. The fluid, which is heated at the left side of the wall is circulating through the opening on the left. Its strength, $\Psi_{max}=154.94$ ($X=0.63$, $Y=0.84$), is reduced with respect to the base case of Fig. 2c. The

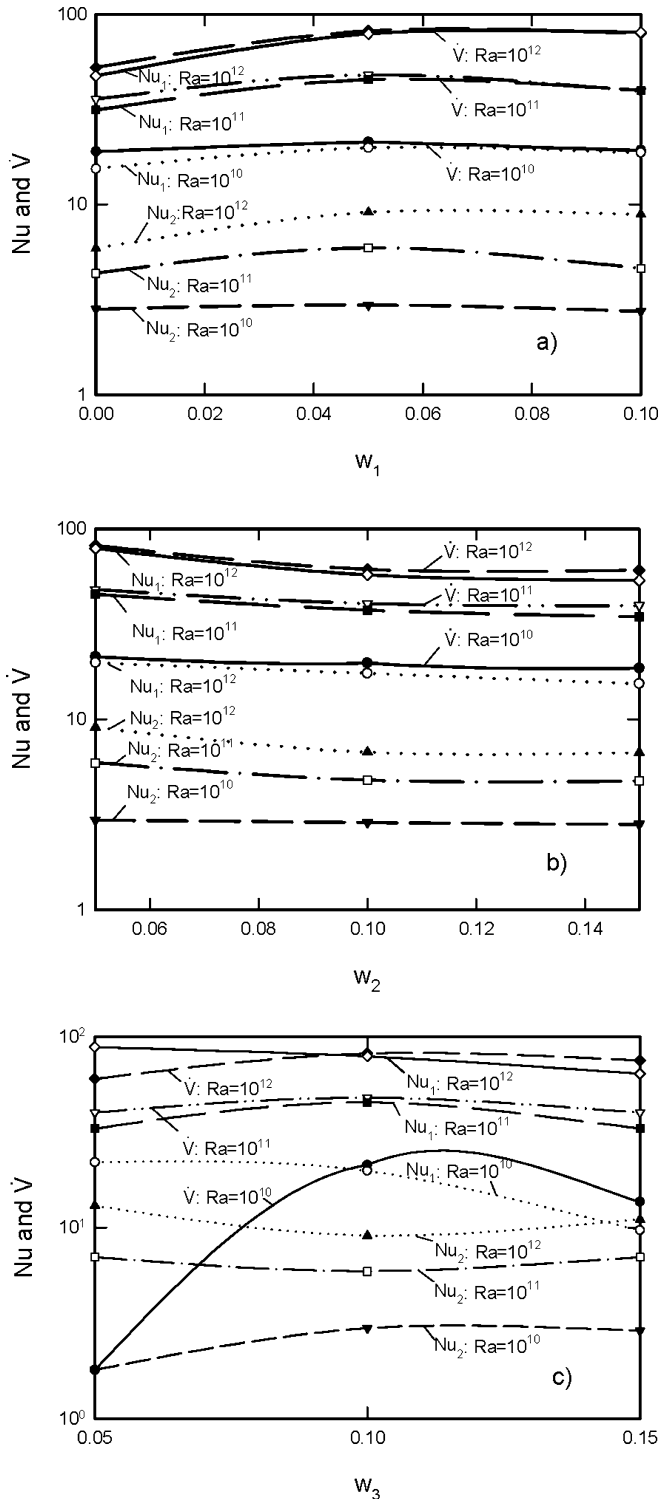


Fig. 7. Normalized Nusselt number and volume flow rate for the base case as a function of a) insulation thickness, w_1 , b) wall thickness, w_2 , c) chimney channel width, w_3 for $Ra = 10^{10}$ to 10^{12}

main clockwise rotating cell is connected to both openings and seems to be responsible with the mass transfer. Its strength is $\Psi_{min} = -94.92$ ($X=0.48$, $Y=0.44$). An additional anti-clockwise rotating cell is formed between the latter and the left boundary. We observe that the fluid flow is choked between the two clockwise

rotating cells. The isotherms on the right of Fig. 8a show steep gradients in the chimney. \dot{V} , Nu_1 , Nu_2 are all lower compared to the base case, which we can see in Fig. 9. When k_r is increased to 10, the streamlines and isotherms in Fig. 8b show basically the same pattern as in the base case with reduced strength of $\Psi_{max} = 236.01$ ($X=0.60$, $Y=0.86$) and $\Psi_{min} = -237.58$ ($X=0.40$, $Y=0.40$), indicating a slightly reduced heat and mass transfer. Indeed, Fig. 9 shows that for $k_r > 10$, \dot{V} , Nu_1 , Nu_2 are not sensitive to it at $Ra = 10^{12}$.

At lower Rayleigh numbers, this trend is different: at $Ra = 10^{10}$, \dot{V} , Nu_1 , Nu_2 are not too sensitive to k_r , but at $Ra = 10^{11}$ they are an increasing function of it when k_r is greater than 10. As expected, the effect of conductivity ratio on the flow rate and heat transfer is felt more when the energy released by the heat source is increased.

11 Effect of enclosure aspect ratio

The aspect ratio was varied from 0.5 to 2.0. Its effect on \dot{V} , Nu_1 and Nu_2 is shown in Fig. 10. We see that the fluid flow rate and heat transfer are all sensitive to the variation of aspect ratio, A . For example, at $Ra=10^{10}$, the flow rate and heat transfer are $\dot{V}=7$, $Nu_1 = 2.25$ at $A=0.5$. They increase and pass through a maximum of 18 and 21 near $A \approx 1$, and then decrease to near 7 and 2.5 at $A=2.0$. Similarly, Nu_2 goes from 1.4 to 3 and then 1.6. We observe similar trends at $Ra=10^{11}$ and $Ra=10^{12}$. It appears that there is an optimum for the aspect ratio near one. The reason is due to reduced convection in the left part of the enclosure: for example at $Ra=10^{11}$, with respect to the base case with $A=1$, the enclosure with $A=0.5$ is twice as high for the same L , and the streamlines showed the anti-clockwise cell was split into two at the upper part near the wall, making the heat transfer difficult. The clockwise cell was pushed upward just below the opening, choking the fluid flow. The strength of circulation was reduced to $\Psi_{max} = 93.45$ ($X=0.24$, $Y=0.91$) and $\Psi_{min} = -54.93$ ($X=0.12$, $Y=0.75$). Consequently both heat and mass transfer is reduced. For $A=2.0$ for the same case, the enclosure height is half of the base case, and the streamlines showed the anti-clockwise cell filling the long enclosure, thus confining the fluid flow near the left boundary and the bottom. The strength of circulation was reduced to $\Psi_{max} = 2354$ ($X=0.13$, $Y=0.16$) and $\Psi_{min} = -11.81$ ($X=0.95$, $Y=0.33$). As a result, the heat and mass transfer is reduced.

12 Conclusion

Conjugate heat transfer by laminar natural convection and conduction in enclosures with openings has been numerically studied for the case of constant heat flux on the chimney wall, isothermal vertical boundaries with openings and horizontal adiabatic boundaries. Equations of mass, momentum and energy have been solved using constant properties and Boussinesq approximation. It is found that (i) Heat transfer, Nu and volume flow rate, \dot{V} are both an increasing function of Rayleigh, Ra , opening height, h_1 at high Ra numbers, orifice height, h_3 , and

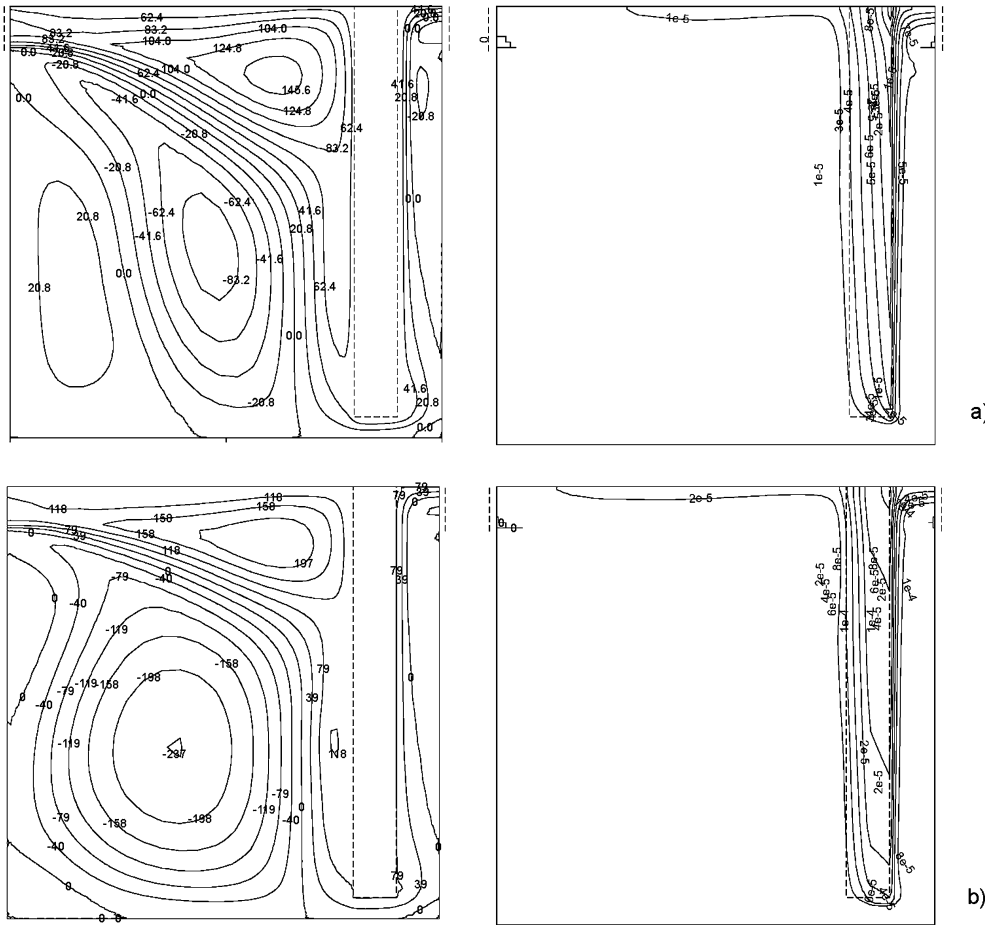


Fig. 8. Streamlines (on the left) and isotherms (on the right) for the base case at $Ra=10^{12}$ with various conductivity ratios, k_r . The composite solid wall in the enclosure is shown with dashed line. The openings on the left, h_1 and on the right, h_2 are shown on the upper part of the enclosure with dashed lines. a) $k_r=1$, b) $k_r=20$

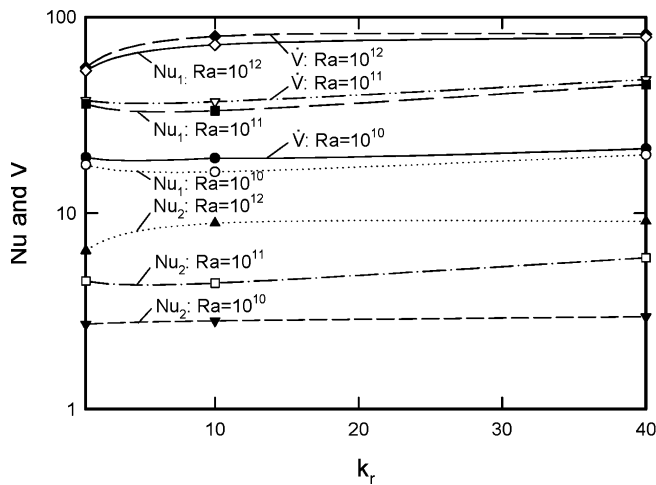


Fig. 9. Normalized Nusselt number and volume flow rate for the base case as a function of conductivity ratio, k_r , for $Ra = 10^{10}$ to 10^{12}

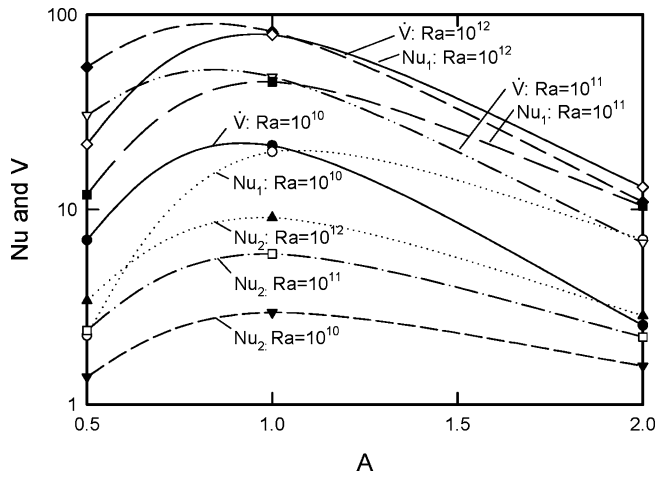


Fig. 10. Normalized Nusselt number and volume flow rate for the base case as a function of aspect ratio, A , for $Ra = 10^{10}$ to 10^{12}

conductivity ratio, k_r , (ii) They are a decreasing function of opening height, h_1 at low Ra numbers, opening height, h_2 , and solid wall thickness, w_2 , (iii) Heat transfer, Nu and volume flow rate, \dot{V} have optima with respect to insulation thickness, w_1 , chimney channel width, w_3 and the aspect ratio, A .

References

1. Gebhart B; Jaluria Y; Mahajan RP; Sammakia B (1988) Buoyancy-induced flows and transport, Hemisphere Publishing Corp, New York
2. Patankar SV (1978) A numerical method for conduction in composite materials, flow in irregular geometries and conjugate heat transfer. Proc 6th Int Heat Transfer Conf vol. 3, pp 279–302

3. Du Z-G; Bilgen E (1992) Coupling of wall conduction with natural convection in a rectangular enclosure. *Int J Heat Mass Transfer*, 35: 1969–1975
4. Mbaye M; Bilgen E (1993) Conduction and convection heat transfer in composite solar collector systems with porous absorber. *Waerme u. Stoffuebertragung* 28: 267–274
5. Prakash C; Kaminski DA (1984) Conjugate natural convection in square enclosure: effect of conduction in one of the vertical walls. *HTD ASME* 39: 49–54
6. Ben Yedder R; Bilgen E (1997) Laminar natural convection in inclined enclosures bounded by a solid wall. *Heat Mass Transfer* 32: 455–462
7. Du S-Q; Bilgen E; Vasseur P (1998) Mixed convection heat transfer in open ended channels with protruding heaters. *Heat Mass Transfer* 34: 265–270
8. Sathe SB; Sammakia BG (2000) A numerical study of the thermal performance of a tape ball grid array (tbga) package. *J Electronic Packaging* 122: 107–114
9. Harman SA; Cole KD (2001) Conjugate heat transfer from a two-layer substrate model of a convectively cooled circuit board. *J Electronic Packaging* 123: 156–158
10. Thrasher WW; Fisher TS; Torrance KE (2000) Experiments on chimney-enhanced free convection from pin-fin heat sinks. *J Electronic Packaging* 122: 350–355
11. Jilani G; Jayaraj S; Voli KK (2001) Numerical analysis of free convective flows in partially open enclosure. *Heat Mass Transfer*. DOI 10.1007/S002310100251/online publication, Nov 29
12. Sayigh AA (1979) (ed) *Solar energy applications in buildings*. Academic Press, New York
13. Ben Yedder R; Bilgen E (1991) Natural convection and conduction in Trombe wall systems. *Int J Heat Mass Transfer* 34: 1237–1248
14. Patankar SV (1980) *Numerical heat transfer and fluid flow*. Hemisphere Publishing Corp, New York
15. Ben Yedder R (1996) *Etude parametrique de la convection laminaire et turbulente dans des espaces clos avec parois solides*, Ph.D. thesis, University of Montreal